fire

MDPI

Article

Improving Fire Suppression Efficiency in Electric Vehicles: A Study on Optimized Upward Spray Devices

Jin-Dong Oh [1], Chan-Hoo Kim [1] and Sung-Young Park [2,*]

[1] Mechanical Engineering Department, Kongju National University, 1223-24, Cheonan-Daero, Seobuk-gu, Cheonan-si 31080, Chungcheongnam-do, Republic of Korea; a20220348@smail.kongju.ac.kr (J.-D.O.); cksgn6543@smail.kongju.ac.kr (C.-H.K.)

[2] Future Automotive Engineering Department, Kongju National University, 1223-24, Cheonan-Daero, Seobuk-gu, Cheonan-si 31080, Chungcheongnam-do, Republic of Korea

* Correspondence: sungyoung@kongju.ac.kr

Abstract: Fire accidents in electric vehicles are mainly caused by battery fires, and one of the most effective fire suppression methods is to spray water from the bottom of a vehicle in an upward direction. In this study, analyses and experiments were conducted to improve the spray angle of a fluidic oscillator used for attaching an upward spray device. Through these analyses, the factors resulting in the maximum spray angle were derived from the four design variables of the fluidic oscillator, which were reconstructed for further analysis. The model that combined the radius of the mixing chamber curvature, inlet wedge width, and outlet wedge width exhibited the largest spray angle (84°) among the combination models that included the outlet wedge width variable. To evaluate the fire suppression performance of the fluidic oscillator nozzle, a cooling-rate comparison experiment was conducted with a recently used orifice nozzle. The results showed that the fluidic oscillator nozzle leads to a faster overall cooling rate than the orifice nozzle, rendering it more suitable for suppressing battery fires. After the production of the upward spray device, practical tests showed that it could spray a large area under a vehicle, thereby suggesting its applicability in actual fire scenes.

Keywords: electric vehicle; battery; thermal runaway; suppression; upward spray device; fluidic oscillator; spray angle

Citation: Oh, J.-D.; Kim, C.-H.; Park, S.-Y. Improving Fire Suppression Efficiency in Electric Vehicles: A Study on Optimized Upward Spray Devices. *Fire* **2024**, *7*, 460. https://doi.org/10.3390/fire7120460

Academic Editor: Jiaqiang E

Received: 23 October 2024
Revised: 20 November 2024
Accepted: 29 November 2024
Published: 6 December 2024

1. Introduction

In recent years, the automotive industry has begun to transition from internal combustion engine vehicles to electric vehicles, owing to growing environmental regulations aimed at slowing climate change [1–3]. Electric vehicles use secondary battery for energy storage, with lithium-ion batteries (LIBs) having the highest energy densities among the available secondary batteries [4–7]. Electric vehicles equipped with LIBs tend to have shorter mileages than conventional internal combustion engine vehicles, and battery manufacturers are conducting several studies to further increase the energy densities of these batteries [8,9]. In addition, LIBs are sensitive to external shock and heat, leading to damage to the internal separator, such as upon heating at temperatures of 130–150 °C. If the separator is damaged, a localized short circuit between the cathode and anode occurs, causing flammable electrolytes to leak out, and leading to ignition and explosion [9–11]. During a fire, the electrolyte inside the battery vaporizes, producing flammable gases such as H_2, CH_4, C_2H_6, and C_2H_4. These flammable gases cause the fire temperature to increase abnormally, leading to thermal runaway in the battery [9,11–15]. Electric vehicle fires mainly originate from battery fires, and despite worldwide research efforts into electric vehicle fire risk assessments and battery fire mechanisms, investigations into fire suppression are limited [16]. Current methods employed to suppress electric vehicle fires involve suffocation with a cover and spraying directly with water. After suppressing the

primary fire, the electric vehicle is immersed in a fire-suppressing tank to prevent reignition and the generation of a secondary fire. However, owing to the fire characteristics of LIBs, suffocating covers are not effective in suppressing the fire, and can only prevent the fire from spreading to the surrounding area. Jeon et al. conducted a fire dynamics simulation to compare fire progression in electric vehicles and internal combustion electric vehicles. The internal combustion electric vehicles did not reach critical risk levels within 600 s, whereas electric vehicles attained critical levels for visibility, temperature, and oxygen concentration at approximately 130, 300, and 500 s, respectively [17]. Ko et al. conducted large-scale fire suppression experiments in underground parking lots, demonstrating that combining upper sprinklers with lower water spray systems reduced thermal runaway in electric vehicle battery packs by approximately 50%. These findings indicate that enhancing existing fire suppression systems can significantly improve their response to electric vehicle fires [18]. According to a study on the response to electric vehicle battery fires in Korea, the most effective method was to spray water from the bottom to the top of the vehicle, leading to improved fire suppression and reduced thermal damage [19]. Galushkin et al. examined the potential for thermal runaway in batteries as a function of their age and outlined the mechanisms behind battery thermal runaway, highlighting the increased risk in older batteries [20]. Additionally, Kim et al. provided a comprehensive review of electric vehicle fire experiments conducted in Korean fire centers and the existing literature, emphasizing key findings that can inform future safety measures [21]. Furthermore, Ha et al. investigated the use of carbon fiber, fiberglass, and silica fiber fabrics in asphyxiation foam for extinguishing electric vehicle fires, demonstrating that carbon fiber fabrics offered superior performance in fire suppression [22]. Lim et al. evaluated various methods for suppressing electric vehicle fires, concluding that certain techniques significantly outperformed others in effectiveness [23]. Liu et al. proposed a water mist method for battery thermal management and fire suppression, showing promising results in cooling performance and the prevention of thermal runaway [24].

In this study, an upward spray device is evaluated which is based on the spraying of water from the underside of a vehicle in the event of an electric vehicle fire, as shown in Figure 1. For this purpose, a fluidic oscillator capable of spraying water over a wide range is employed, and an internal geometry optimization study is conducted to apply the fluidic oscillator. The fluidic oscillator possesses a symmetrical structure with feedback channels on the left and right sides of the mixing chamber (Figure 2), which generates regular oscillations in the atomized flow. Notably, the atomization characteristics of fluidic oscillators are difficult to develop because they are strongly affected by small changes in the internal geometry variables [25–27]. Therefore, in this study, the fluidic oscillator is optimized for application in an upward spray device by means of various analytical and experimental approaches. Traditional methods for extinguishing electric vehicle fires involve preventing fire spread by spraying water from a distance or using a fire blanket. However, this study focuses on direct cooling of batteries to enhance cooling speed and fire suppression efficiency. Analytical and experimental techniques were used to optimize the fluidic oscillator's design, ensuring practicality in the limited space under the vehicle.

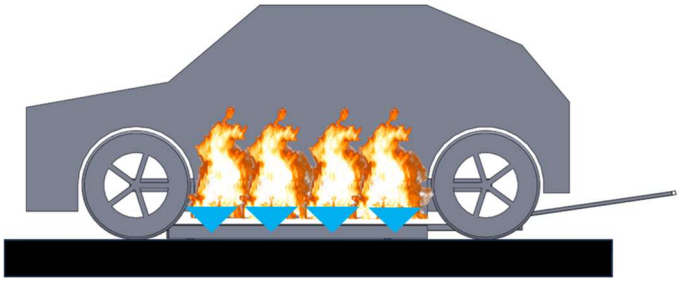

Figure 1. Concept design for fire suppression using an upward spray device.

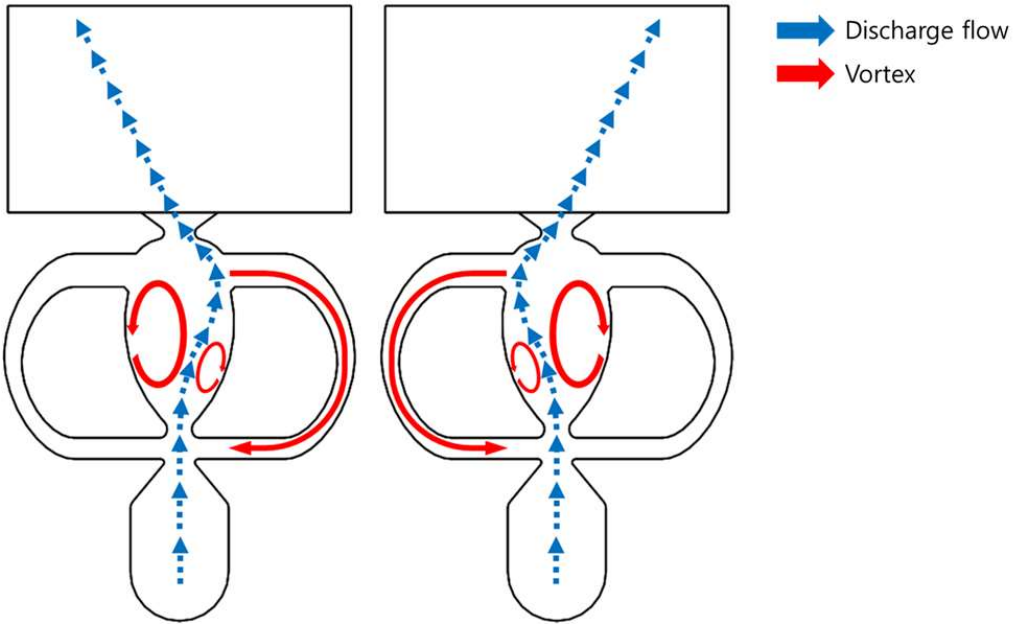

Figure 2. Operation principles of the fluidic oscillator.

2. Materials and Methods

2.1. Design Variables

To optimize the exit spray angle and oscillation period of the fluidic oscillator of the upward spray device to suppress electric vehicle battery fires, the internal design parameters were selected based on previous studies [25,26]. The nozzle height was set to 70 mm to accommodate the minimum ground clearance of the vehicle (i.e., 100 mm). The design variables (MR, IW, OR, and OW) are shown and defined in Figure 3, while the dimensions of the design variables are listed in Table 1. The spray angle and oscillation period were analyzed for a total of 24 models.

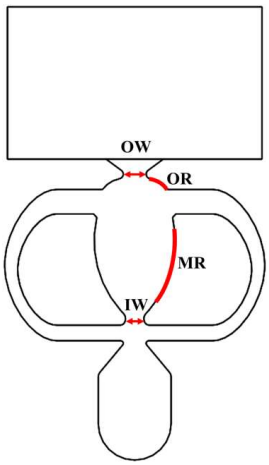

(**a**)

Variable	Explanation
MR	Radius of the mixing chamber curvature
IW	Inlet wedge width
OR	Radius of the outlet curvature
OW	Outlet wedge width

(**b**)

Figure 3. (**a**) Schematic representation of the design variables. (**b**) Definitions of the various design variables.

Table 1. Dimensions of the design variables employed in the current model.

Model	MR [mm]	IW [mm]	OR [mm]	OW [mm]
Base	20.7	3.60	5.11	4.50
MR-0.93	19.25			
MR-0.97	20.00			
MR-0.98	20.30			
MR-1.01	21.00			
MR-1.02	21.10			
IW-0.88	20.70	3.15		
IW-0.94		3.38		
IW-1.06		3.80		
IW-1.11		4.00		
IW-1.18		4.25		
IW-1.24		4.46		
IW-1.30		4.68		
OR-0.98		3.60	5.00	
OR-1.04			5.30	
OR-1.08			5.50	
OR-1.12			5.70	
OW-0.89			5.11	4.00
OW-0.96				4.30
OW-1.04				4.70
OW-1.11				5.00
OW-1.16				5.22
OW-1.20				5.40
OW-1.24				5.58

2.2. Analytical Conditions and Calculation Grid

Flow analysis of the fluidic oscillator nozzle was performed using the commercial analysis program Star-CCM+, and the SST k-Ω turbulence model was used for three-dimensional transient flow analysis [28]. The mesh conditions are listed in Table 2. The flow domain of the generated mesh is shown in Figure 4, and the number of elements generated was ~80,000. The time step for the unsteady-state flow analysis was calculated to be 2.5×10^{-5} s, considering the CFL number, the mesh size, and the fluid velocity.

Table 2. Mesh conditions.

Parameter	Unit	Value
Mesh type	-	Polyhedral
Base size	mm	0.8
Number of prism layers	-	5
Prism layer thickness	mm	0.26
Prism layer stretching	-	1.5
Minimum surface size	mm	0.08

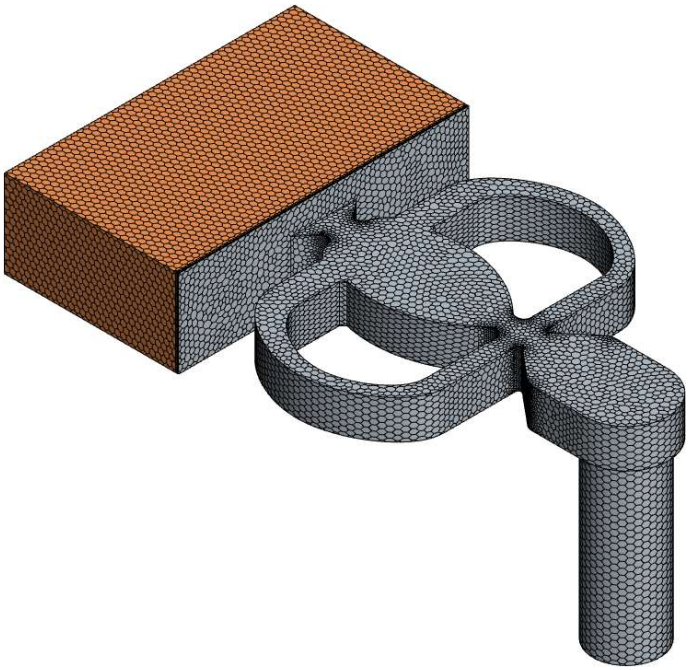

Figure 4. Three-dimensional model of the fluidic oscillator for simulation purposes.

The fluid used for analysis was water with a density of 997 kg/m^3 and a viscosity of 0.000887 Pa·s. Considering the water pressure used in the upward spray device, the inlet was set to a gauge pressure of 5.0 bar, and the outlet was set to atmospheric pressure.

3. Results and Discussion

3.1. Analytical Results

The upward spray device operating from the vehicle's underside works within a limited space of 100 mm (the minimum ground clearance regulation). To overcome this restricted operating space, it is necessary to widen the spray angle of the fluidic oscillator attached to the upward spray device. The spray angle determines the spray area and cooling efficiency. Therefore, it is essential to identify the changes in the exit spray angle of the fluidic oscillator based on internal design variables. The results of the flow analysis for the various design variables are shown in Figures 5 and 6. More specifically, Figure 5 shows the measured spray angle for each design variable, while Figure 6 shows the velocity field for the model with the maximum spray angle calculated for each design variable. For the MR variable, the MR-0.97 model had the largest spray angle of 68°, beyond which the spray angle decreased sharply, reaching 0° in the MR-1.02 model. It is believed that the vortices generated simultaneously on the left and right walls inside the mixing chamber blocked the entrance to the feedback channel, preventing vibrations from occurring. For the IW variable, the IW-1.18 model gave the largest spray angle of 71°, while for the OR variable, OR-1.08 exhibited the largest spray angle of 62°. Notably, the OR-0.98 model gave a spray angle of 0° and did not generate oscillations for reasons similar to those described for the MR-1.02 model. With the exception of the OR-0.98 model, the variation in the spray angle was within 10°, indicating that the OR variable did not significantly affect the spray angle. For the OW variable, the OW-1.16 model exhibited the largest spray angle of 63°. Between the OW-0.89 and OW-1.16 model, the spray angle increased as the OW increased, reaching its maximum value, and declining for subsequent OW models.

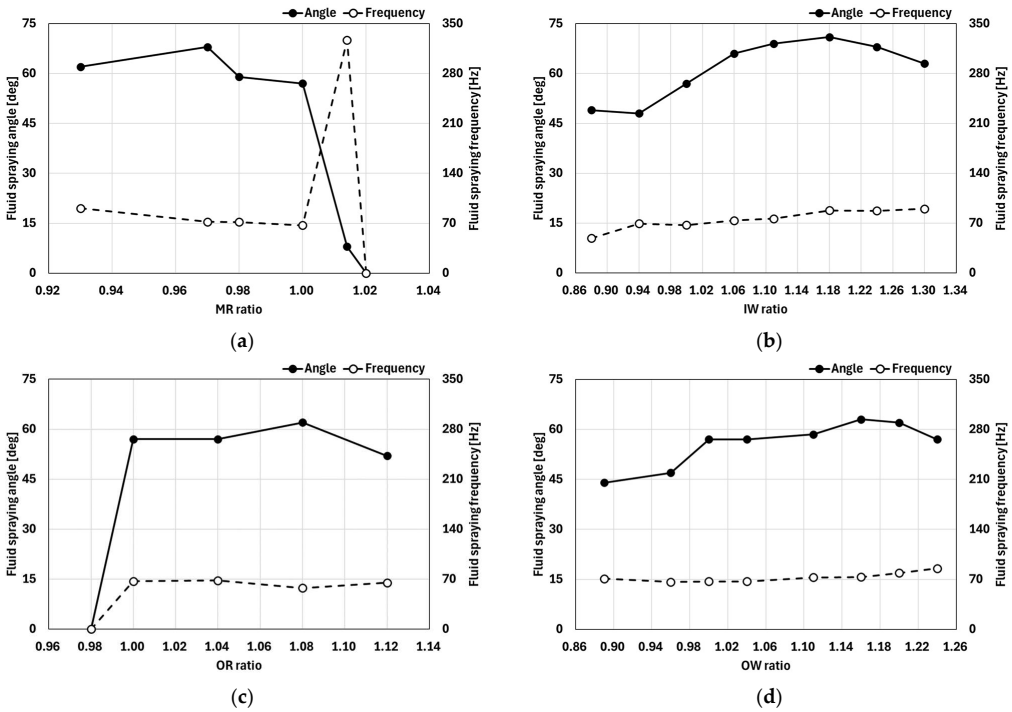

Figure 5. Results of the fluid spray angle and frequency experiments for the (**a**) MR model, (**b**) IW model, (**c**) OR model, and (**d**) OW model.

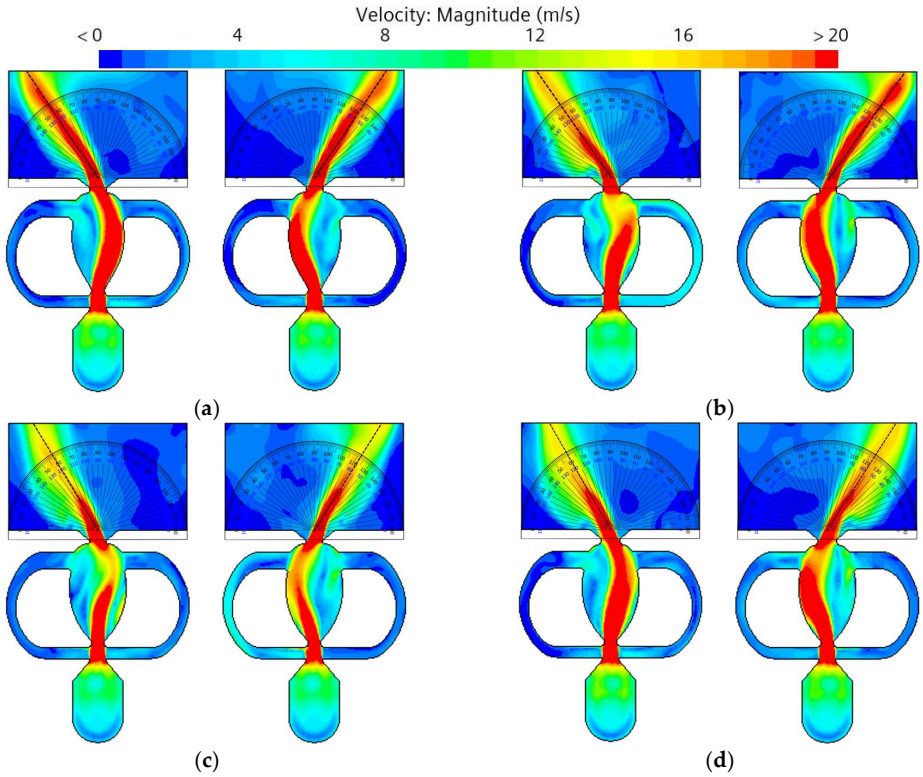

Figure 6. Results of the maximum spray angle for the (**a**) MR-0.97, (**b**) IW-1.18, (**c**) OR-1.08, and (**d**) OW-1.16 models.

3.2. Analysis of Nozzle Optimization

The factors affecting the maximum spray angles were further analyzed by their reconstruction from the four design variables of the fluidic oscillator. The combinations of these design variables are listed in Table 3. Eleven additional models were designed

and analyzed, and the obtained results were used to explain the correlation between the design variables.

Table 3. Model design variable combinations.

Combination	MR [mm]	IW [mm]	OR [mm]	OW [mm]
MR + IW	20.00	4.25	5.11	4.50
MR + OR	20.00	3.60	5.50	4.50
MR + OW	20.00	3.60	5.11	5.22
IW + OR	20.70	4.25	5.50	4.50
IW + OW	20.70	4.25	5.11	5.22
OR + OW	20.70	3.60	5.50	5.22
MR + IW + OR	20.00	4.25	5.50	4.50
MR + IW + OW	20.00	4.25	5.11	5.22
IW + OR + OW	20.70	4.25	5.50	5.22
MR + OR + OW	20.00	3.60	5.50	5.22
MR + IW + OR + OW	20.00	4.25	5.50	5.22

The results of the combined model analysis are shown in Figure 7, while Figure 8 shows the spray angle results obtained for the three models that exhibited the best spray angles among the combined model analysis results (i.e., MR + OW, IW + OW, and MR + IW + OW). The MR + IW + OW model exhibited the highest spray angle of 84°, followed by the MR + OW and IW + OW models at 80.5 and 79°, respectively. To determine the correlation between different design variable combinations, the obtained results were analyzed by scoring on a scale of 1–5 based on the spray angle range, as shown in Figure 7b. The sum of the scores in the vertical rows shows that OW scored the highest, with a total score of 28. The MR and IW variables scored second highest at 22 in both cases, while the OR variable scored lowest at 16. It was also found that the OW design variable improved the spray angle to the greatest extent when combined with the MR and IW design variables, while the MR and IW design variables did not improve the spray angle when not combined with the OW design variable. In addition, the OR design variable scored lowest when combined with the MR, IW, and OW design variables. The OR variable also reduced the spray angle when combined with the MR + OW, IW + OW, and MR + IW + OW models, which yielded the highest spray angles. These results indicate that the OR design variable reduced the effectiveness of the spray angle improvement.

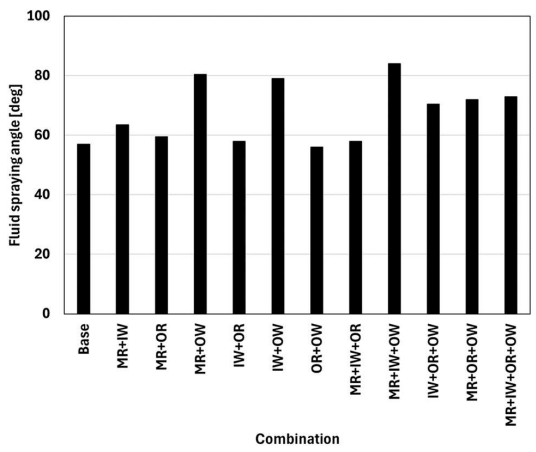

(**a**)

	MR	IW	OR	OW
MR	-	2	1	5
IW	2	-	1	5
OR	1	1	-	1
OW	5	5	1	-
MR+IW	-	-	1	5
MR+OR	-	1	-	4
MR+OW	-	5	4	-
IW+OR	1	-	-	4
IW+OW	5	-	4	-
OR+OW	4	4	-	-
MR+IW+OR	-	-	-	4
MR+IW+OW	-	-	4	-
MR+OR+OW	-	4	-	-
IW+OR+OW	4	-	-	-
Total Score	22	22	16	28

Score	Spray angle	Mean
5	75 ~	Excellent
4	70 ~ 75	Good
3	65 ~ 70	Average
2	60 ~ 65	Not Bad
1	0 ~ 60	Bad

(**b**)

Figure 7. (**a**,**b**) Simulation results according to the different variable combinations, and the spray angle results.

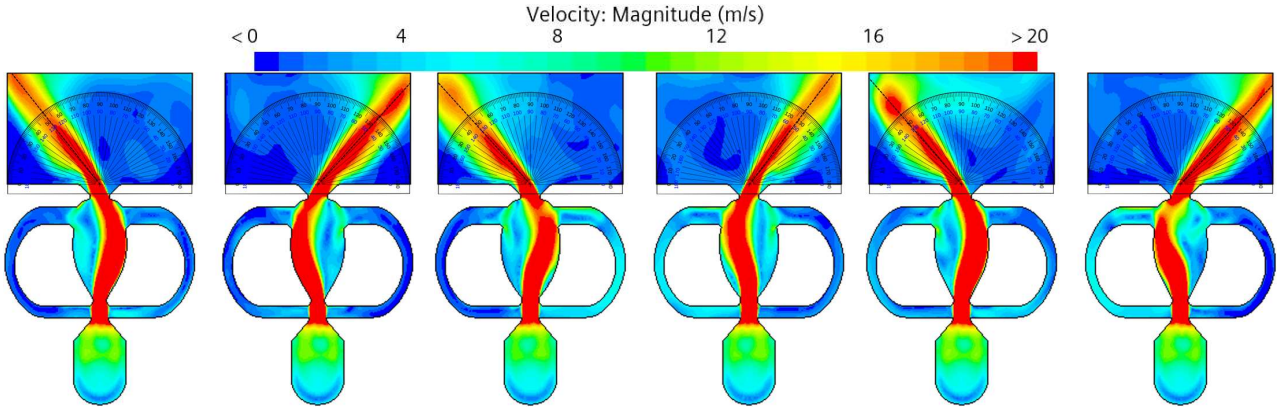

Figure 8. Spray angle results according to the different variable combinations: (**a**) MR + OW, (**b**) IW + OW, and (**c**) MR + IW + OW.

3.3. Nozzle Spray Experiments

The design of the fluidic oscillator was based on an in-house research patent [29]. A regulation requires a minimum ground clearance of 100 mm for the vehicle underbody. Given that commercial vehicles typically have a ground clearance of 170–180 mm, the oscillator's height was limited to 70 mm. For manufacturing, precision machining was performed by an external institution using a five-axis computer-numerical-control process. To ensure the reliability of the analysis, a schematic diagram of the experiment was drawn, as shown in Figure 9a, and a fluidic oscillator experimental apparatus was constructed, as presented in Figure 9b. The pump employed in this experiment discharged water at a pressure of up to 3 bar, as measured using a manometer. Thus, two pumps were connected in series to ensure a stable supply, and the water pressure was regulated using a pressure-regulating valve. To compare the experimental and analytical conditions, the water pressure and mass flow rate were set at ~5 bar and ~0.5 kg/s, respectively.

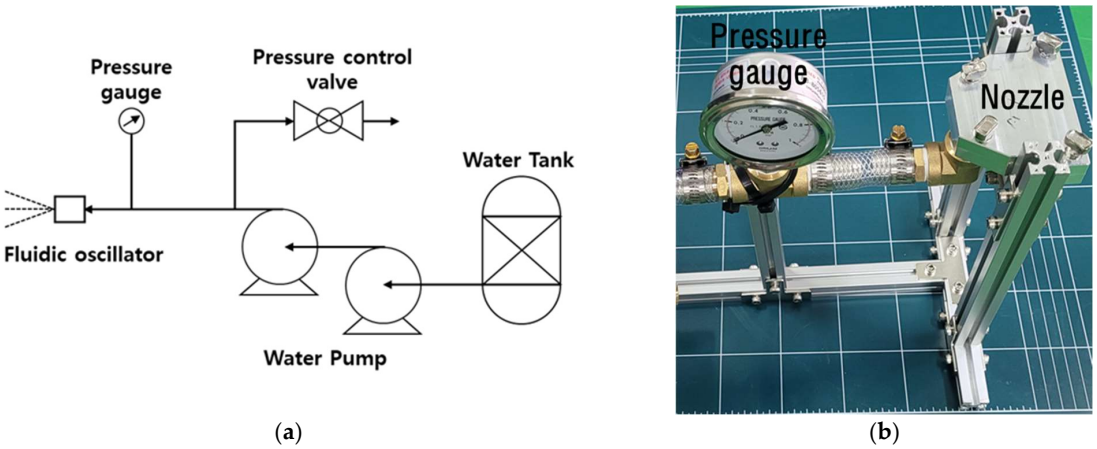

Figure 9. The fluidic oscillator nozzle experiment rig: (**a**) schematic representation, and (**b**) photographic image.

The experimental results obtained for the spray angle experiments are shown in Figure 10 for the base model, the MR + OW model, the IW + OW model, and the MR + IW + OW model. The spray angle measurement was based on the center of the sprayed fluid close to the outlet, considering the shooting time and side-to-side movement of the fluid. Consequently, the spray angle was measured to be 53° for the base model, 76° for the MR + OW model, 77° for the IW + OW model, and 82° for the MR + IW + OW model.

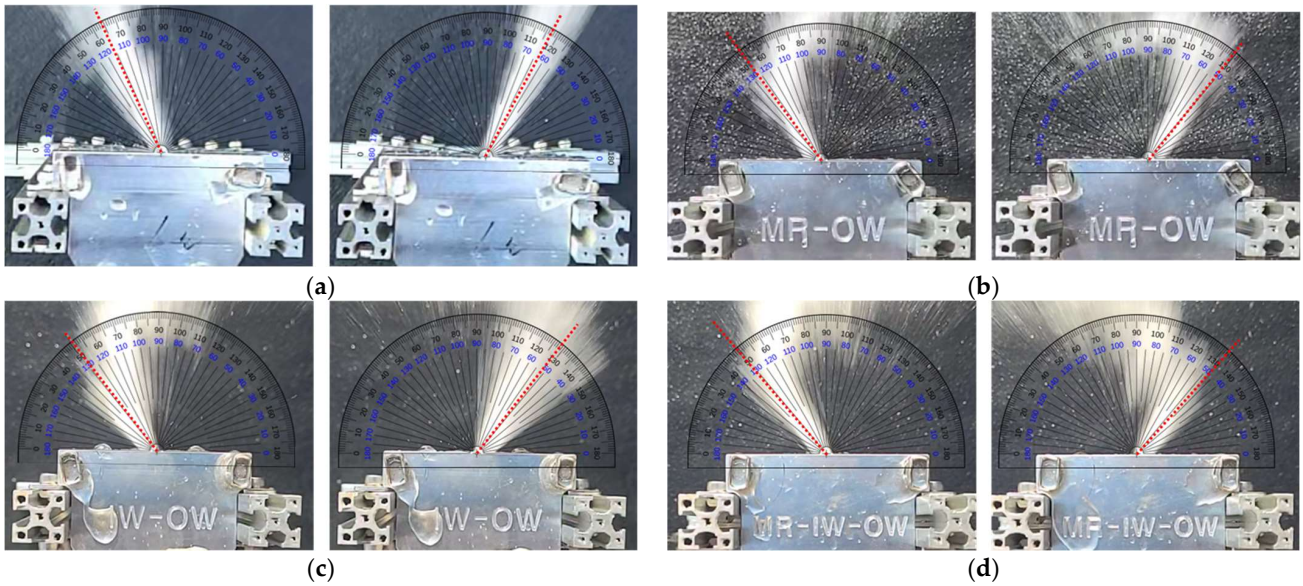

Figure 10. Experiment results for the fluid spray angle. (**a**) The base model, (**b**) the MR + OW model, (**c**) the IW + OW model, and the (**d**) MR + IW + OW model.

Table 4 and Figure 11 present a comparison of the simulated and experimental spray angle results, wherein it can be seen that the experimental values were lower than the simulated values. The errors calculated between the simulated and experimental results were 7.02% for the base model, 5.59% for the MR + OW model, 2.53% for the IW + OW model, and 2.38% for the MR + IW + OW model, thereby confirming the reliability of the simulated results. In addition, both the simulated and experimental results showed that the MR + IW + OW model gave the largest spray angle, indicating that it is suitable for use as a fluidic oscillator model in upward spray devices.

Table 4. Comparison of the experimental and simulated results.

Model	Simulation [°]	Experimental [°]	Error [%]
Base	57	53	7.02
MR + OW	80.5	76	5.59
IW + OW	79	77	2.53
MR + IW + OW	84	82	2.38

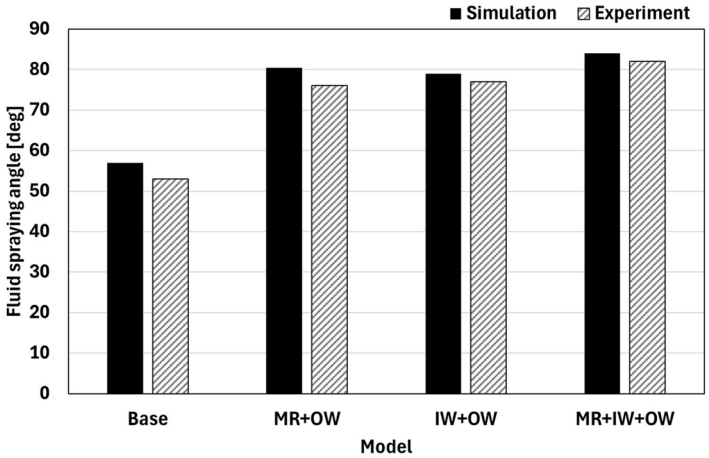

Figure 11. Comparison of the experimental and simulated spray angle results.

3.4. Fluidic Oscillator Cooling Performance

The upward spray device for suppressing electric vehicle battery fires, introduced in the press release by the National Fire Agency, is of the orifice nozzle (ON) type, which utilizes holes drilled into a pipe [17]. A cooling performance experiment was conducted to compare the fire suppression performances of orifice and fluidic oscillator nozzles (FONs). The ON manufacturing method involved creating a hole in a square pipe with an area equal to that of the FON outlet. Experiments were conducted by supplying the same flow rate. Figure 12a shows the heating plate of the experimental device, to which three 283 W heating rods are attached. Temperature measurements of the heating plate were performed by attaching eight temperature sensors, as shown in the figure. The heating plate was cooled by spraying water from the bottom, and insulation was employed to prevent heat loss from the top. The models shown in Figure 12b,c were designed to compare the performances of the FON- and ON-type spray devices with equal outlet areas. All experiments were performed with a fluid spray pressure of 4 bar, and the performance evaluation was conducted five times for each spray method.

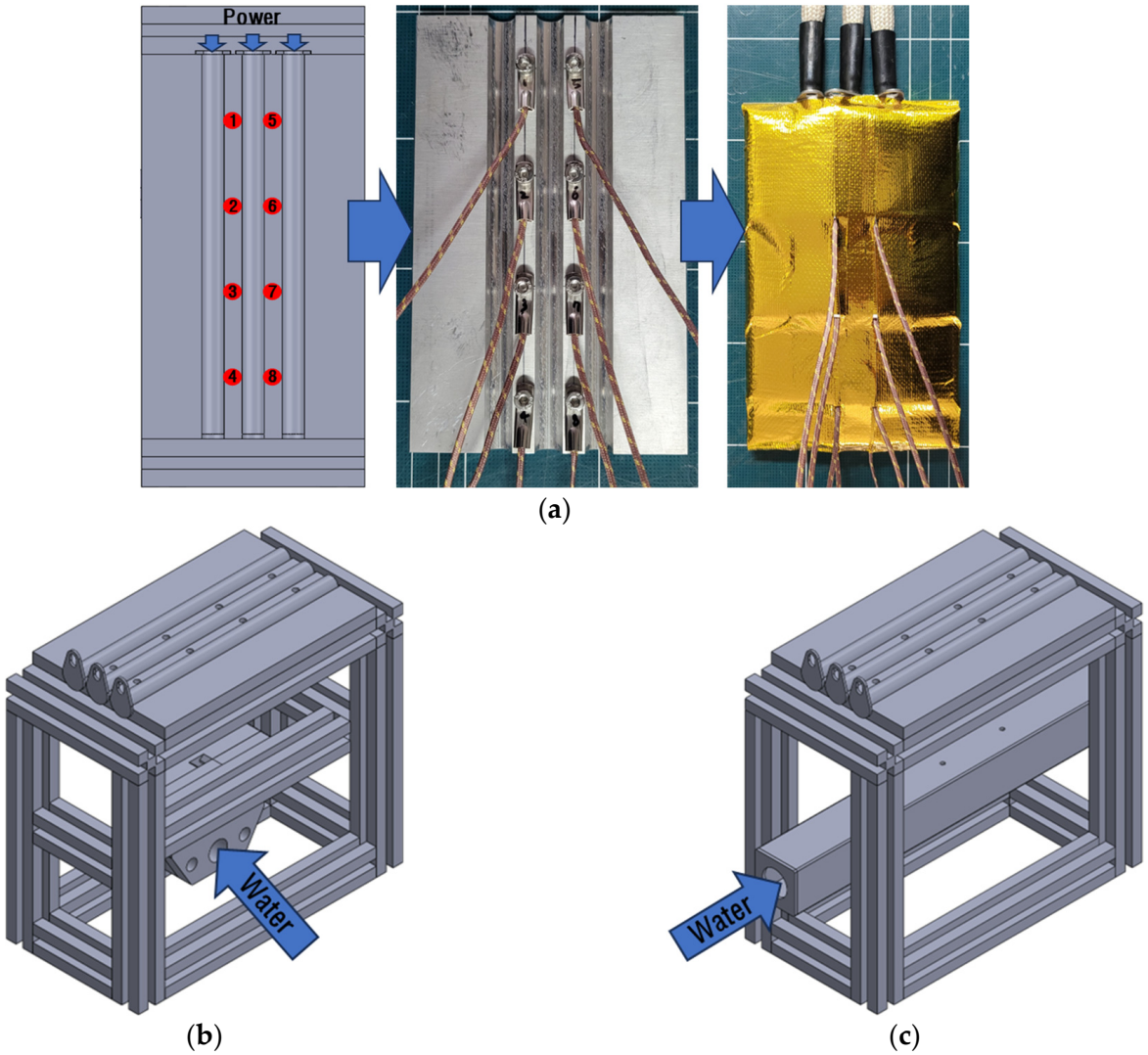

Figure 12. The nozzle cooling performance test device: (**a**) heating plate, (**b**) FON cooling model, and (**c**) ON cooling model.

In this study, a K-type temperature sensor was used for temperature monitoring. The sensor was connected to a Yokogawa data logger DS600 to collect real-time temperature data. Prior to the experiments, the temperature sensor was calibrated by comparing it with

a reference thermometer. The calibration procedure involved measuring sensor values over a range of temperatures and comparing them with a standard instrument. The temperature measurement method for the experiments involved conducting five trials under the same conditions and averaging the three data points, excluding the highest and lowest temperatures, to derive the results.

Figure 13 shows the average temperatures recorded at positions 2, 3, 6, and 7 for the FON and ON systems to compare their cooling performances at the center of the heating plate. The time required to reach 100 °C and the change in temperature over time (dT/dt) were compared. It was found that for the FON spray method, a temperature of 100 °C was reached after 33.25 s, while a significantly longer time of 89.75 s was required using the ON spray method. Similarly, upon comparing the dT/dt values for reaching a temperature of 100 °C, cooling rates of −9.77 and −3.62 °C/s were obtained for the FON and ON systems, respectively. These differences can be accounted for by considering that the FON sprays fluid to the left and right, resulting in the injected water droplets hitting the bottom of the heating plate, and generating a stagnation point. This resulted in a high initial cooling rate due to the large heat transfer coefficient. In contrast, for the ON system, water is continuously injected into the same location and a fluid film is formed under the heating plate to prevent the fluid from directly contacting the heating plate; therefore, the heat transfer coefficient may be lower than that achieved using the FON spray.

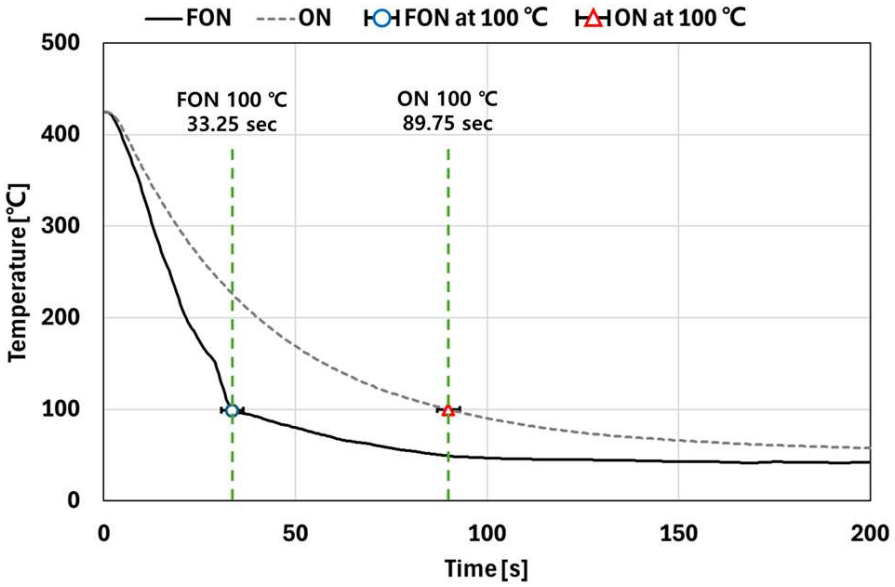

Figure 13. Average temperature changes on the heating plate.

3.5. Development of an Upward Spray Device

A three-dimensional (3D) model of an upward spray device was subsequently designed for use in fire suppression, as outlined in Figure 14a. For this purpose, a 70 × 70 mm angular pipe was employed, and a fluidic oscillator for the side branch was designed by tilting it 25° to widen the spray range. Calculations indicated that by equipping the upward spray device with MR + IW + OW nozzles, tilted at an angle of 25°, water could be effectively sprayed over an area of approximately 830 mm (width) × 500 mm (length) under a vehicle with a minimum ground clearance of 170 mm. A ball valve and a one-touch connector were applied at the inlet to allow the rapid and facile installation of the fire nozzle. The total length of the upward spray device, which was designed to be mounted in the loading box of the fire truck, was 740 mm. Figure 14b shows a photographic image of the manufactured upward spray device, wherein the connecting parts of the pipes were welded to prevent leakage.

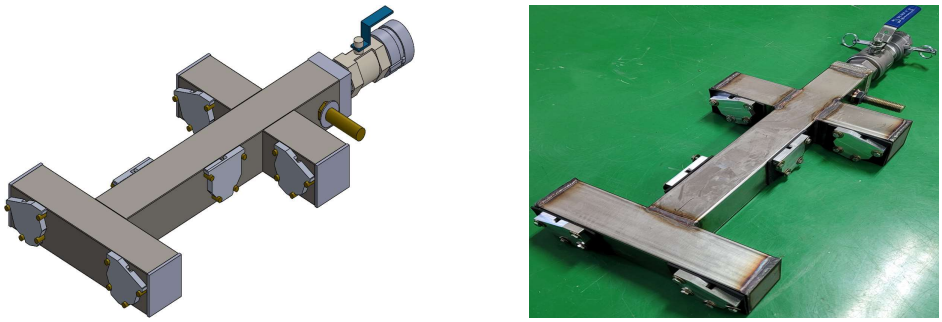

(**a**) (**b**)

Figure 14. Upward spray device to suppress electric vehicle battery fires: (**a**) 3D model and (**b**) manufactured device.

A performance test was subsequently conducted on actual vehicles using the upward spray device. More specifically, the hose of the fire hydrant was connected to the upward spray device using a one-touch connector; this was typically achieved within 20 s. Photographic images recorded outside and under the vehicle during the spray experiment are shown in Figure 15. It can be seen that the wide spray angle of the FON system allowed water to be sprayed over most of the vehicle width. In the event of an actual vehicle battery fire, it would therefore be expected that this system would suppress the fire by preventing its spread and continuously cooling the fire area.

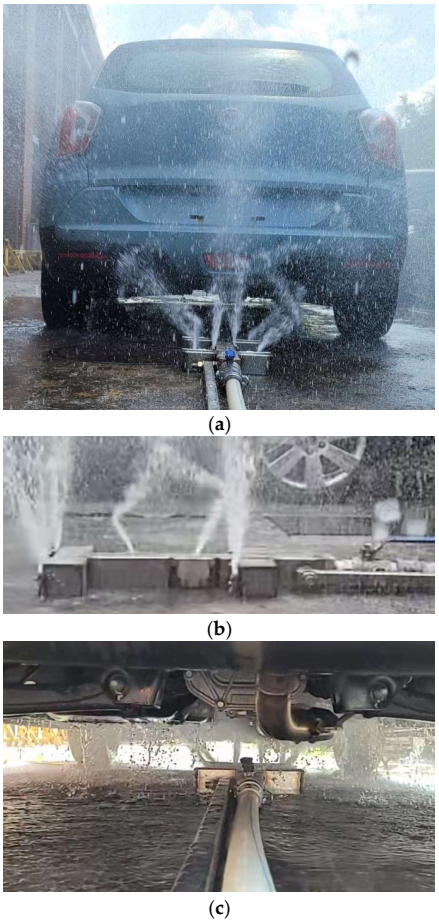

(**a**)

(**b**)

(**c**)

Figure 15. Performance evaluation of the upward spray device. (**a**) Rear view of the spray from outside the vehicle, (**b**) side view of the spray from outside the vehicle, and (**c**) rear view of the spray from under the vehicle.

4. Conclusions

In this study, various design parameters were analyzed to optimize the spray performance of a fluidic oscillator for an upward spray device aimed at suppressing electric vehicle battery fires. The outlet wedge width (OW) was found to be the most effective variable in enhancing the spray angle, with maximum spray angles calculated for each design variable. The MR + IW + OW model (mixing chamber radius and inlet wedge width) achieved the largest spray angle. An experiment revealed that the fluidic oscillator nozzle (FON) had a cooling rate 2.7 times greater than that of the orifice nozzle (ON) when cooling from 425 °C to 100 °C, attributed to its ability to generate a stagnation point over a wide area, thus improving the heat transfer coefficient. The practical application of the fluidic oscillator with a fire truck demonstrated effective water dispersion over a large area beneath the vehicle, indicating potential for real-world fire scenarios.

This study investigated the practicality of an upward spray device using a fluidic oscillator nozzle, setting the device height at 70 mm. Future research will be needed to further develop the device to reduce its height. The upward spray device developed in this study features a long metal handle for insertion under a vehicle. Studies and media reports indicate that flammable gases from electric vehicle battery fires can cause secondary damage, posing significant risks to firefighters. Future studies should focus on integrating an autonomous driving system into the spray device, enabling it to approach the vehicle underbody and extinguish fires automatically. This innovation is expected to reduce firefighter risks and enhance fire-suppression efficiency, thereby improving the safety and practicality of fire response systems for electric vehicle fires.

Author Contributions: Software, J.-D.O.; Validation, J.-D.O. and C.-H.K.; Investigation, J.-D.O.; Writing—original draft, J.-D.O.; Writing—review and editing, C.-H.K. and S.-Y.P.; Supervision, S.-Y.P.; Project administration, S.-Y.P. All authors have read and agreed to the published version of the manuscript.

Funding: This research was supported by a Korea Basic Science Institute (National Research Facilities and Equipment Center) grant funded by the Ministry of Education (Grant No. 2020R1A6C101A187).

Data Availability Statement: The original contributions presented in the study are included in the article, further inquiries can be directed to the corresponding authors.

Conflicts of Interest: The authors declare that this research was conducted in the absence of commercial or financial relationships that could be construed as potential conflicts of interest. This paper was written by organizing and supplementing Jindong Oh's master's thesis.

References

1. Na, Y.U.; Kim, J.S. A study on the characteristic of electric vehicle fire in Korea. In Proceedings of the Fall Academic Conference, Jecheon, Republic of Korea, 17 November 2022.
2. Kim, W.Y. Numerical Analysis on Thermal Runaway in Cylindrical Lithium-Ion Batteries for Electric Vehicles. Master's Thesis, Jeju National University, Jeju, Republic of Korea, 2021.
3. Jung, D.Y. BMS technology for electric vehicles. *Korean Inst. Power Electron.* **2014**, *19*, 45–54.
4. Dong, Y.; Meng, J.; Sun, X.; Zhao, P.; Sun, P.; Zheng, B. Experimental Study on Effects of Triggering Modes on Thermal Runaway Characteristics of Lithium-Ion Battery. *World Electr. Veh. J.* **2023**, *14*, 270. [CrossRef]
5. Yu, W.; Guo, Y.; Xu, S.; Yang, Y.; Zhao, Y.; Zhang, J. Comprehensive recycling of lithium-ion batteries: Fundamentals, pretreatment, and perspectives. *Energy Storage Mater.* **2022**, *54*, 172–220. [CrossRef]
6. Lai, X.; Yi, W.; Cui, Y.; Qin, C.; Han, X.; Sun, T.; Zhou, L.; Zheng, Y. Capacity estimation of lithium-ion cells by combining model-based and data-driven methods based on a sequential extended Kalman filter. *Energy* **2020**, *216*, 119233. [CrossRef]
7. Liu, L.; Xu, J.; Wang, S.; Wu, F.; Li, H.; Chen, L. Practical evaluation of energy densities for sulfide solid-state batteries. *eTransportation* **2019**, *1*, 100010. [CrossRef]
8. Choi, G.W.; Jang, S.M.; Kim, H.B. A study on the risk of fire and fire pattern in secondary cell battery (Li-ion battery). *JFISK* **2018**, *9*, 49–67.
9. Feng, X.; Ouyang, M.; Liu, X.; Lu, L.; Xia, Y.; He, X. Thermal runaway mechanism of lithium ion battery for electric vehicles: A review. *Energy Storage Mater.* **2018**, *10*, 246–267. [CrossRef]
10. Lim, S.H.; Lee, G.Y.; Kim, N.H.; Kim, D.E.; Kil, G.S. Detection and analysis of discharge pulses by failure mechanisms of the separator inside lithium-ion batteries. *J. Korean Inst. Electr. Electron. Mater. Eng.* **2021**, *34*, 327–332. [CrossRef]

11. Xu, B.; Lee, J.; Kwon, D.; Kong, L.; Pecht, M. Mitigation strategies for Li-ion battery thermal runaway: A review. *Renew. Sustain. Energy Rev.* **2021**, *150*, 111437. [CrossRef]
12. Spotnitz, R.; Franklin, J. Abuse behavior of high-power, lithium-ion cells. *J. Power Sources* **2003**, *113*, 81–100. [CrossRef]
13. Finegan, D.P.; Scheel, M.; Robinson, J.B.; Tjaden, B.; Hunt, I.; Mason, T.J.; Millichamp, J.; Di Michiel, M.; Offer, G.J.; Hinds, G.; et al. In-operando high-speed tomography of lithium-ion batteries during thermal runaway. *Nat. Commun.* **2015**, *6*, 6924. [CrossRef] [PubMed]
14. Wen, J.; Yu, Y.; Chen, C. A Review on Lithium-Ion Batteries Safety Issues: Existing Problems and Possible Solutions. *Mater. Express* **2012**, *2*, 197–212. [CrossRef]
15. Guo, G.; Long, B.; Cheng, B.; Zhou, S.; Xu, P.; Cao, B. Three-dimensional thermal finite element modeling of lithium-ion battery in thermal abuse application. *J. Power Sources* **2009**, *195*, 2393–2398. [CrossRef]
16. Chae, G.E.; Park, Y.K.; Choi, J.H. International and domestic electric vehicle fire test research trend survey. In Proceedings of the Spring Academic Conference, Jeju, Republic of Korea, 27 April 2022.
17. Jeon, C.H.; Kim, D.K. Analysis of fire development patterns and risk factors in case of electric vehicle fire in special space (un-derground parking lot). In Proceedings of the Summer Conference, Pyeongchang, Republic of Korea, 22 June 2022.
18. Ko, B.Y.; Yoo, S.H.; Choi, D.H.; Han, K.I. Full-Scale Fire Extinguishing Experiments to Analyze the Adaptability of Firefighting Facilities for Electric Vehicle Fires in Underground Parking Lots in Lithium-ion Battery Fires. *KFSE* **2024**, *38*, 1–8.
19. Korea National Fire Research Institute. Available online: https://www.nfa.go.kr/nfa/publicrelations/policyarchive/promotion/;jsessionid=xui0beuao7Pize62BiY+eXuH.nfa22?boardId=bbs_0000000000000805&mode=view&cntId=66&category=&pageIdx=&searchCondition=&searchKeyword= (accessed on 24 August 2023).
20. Galushkin, N.E.; Yazvinskaya, N.N.; Galushkin, D.N. Mechanism of Thermal Runaway in Lithium-Ion Cells. *J. Electrochem. Soc.* **2018**, *165*, A1303–A1308. [CrossRef]
21. Kang, S.W.; Lee, K.M.; Kwon, M.J.; Choi, J.Y. Examination and proposal for standard operating procedure (SOP) to respond to battery electric vehicle (BEV) fire Incidents. In Proceedings of the Fall Academic Conference, Daegu, Republic of Korea, 25 November 2021.
22. Ha, T.-W.; Park, P.-K. The Study on Next-generation Fire Blanket for Electric Vehicle Fires. *Korean J. Hazard. Mater.* **2023**, *11*, 42–48. [CrossRef]
23. Lim, O.K.; Kang, S.; Kwon, M.; Choi, J.Y. Full-scale Fire Suppression Tests to Analyze the Effectiveness of Existing Lithium-ion Battery Fire Response Procedures for Electric Vehicle Fires. *Fire Sci. Eng.* **2021**, *35*, 21–29. [CrossRef]
24. Liu, T.; Tao, C.; Wang, X. Cooling control effect of water mist on thermal runaway propagation in lithium ion battery modules. *Appl. Energy* **2020**, *267*, 115087. [CrossRef]
25. Moon, H.S. Unsteady computational fluid analysis of fluid vibration characteristics of windshield spray nozzle. Master's Thesis, Kongju National University, Gongju, Republic of Korea, 2020.
26. Choi, J.H. Experimental and Analytical Study on the Internal Flow Characteristics of Windshield Spray Nozzle According to Design Variables. Master's Thesis, Kongju National University, Kongju, Republic of Korea, 2021.
27. Kim, C.-H.; Choi, J.-H.; Park, S.-Y. Performance Development of Fluidic Oscillator Nozzle for Cleaning Autonomous-Driving Sensors. *Appl. Sci.* **2024**, *14*, 1596. [CrossRef]
28. CD-Adapco. Star-CCM+ver. 12.04 User Guide (2017). Available online: https://docs.sw.siemens.com/documentation/external/PL20200805113346338/en-US/userManual/userguide/html/index.html#page/STARCCMP/GUID-7DED1D9B-AAA1-48D4-93A0-62B176764E35.html (accessed on 31 August 2020).
29. Park, S.Y. Apparatus for Oscillating Fluid Injection. Korea. Patent 10-2273574, 30 June 2021.